PNAS RESEARCH ARTICLE | CHEMISTRY

Nanoscale engineering of gold particles in 18th century Böttger lusters and glazes

Celia S. Chari[a], Zane W. Taylor[a], Anikó Bezur[b], Sujing Xie[c], and Katherine T. Faber[a,c,1]

Edited by Admir Masic, Massachusetts Institute of Technology, Cambridge, MA; received November 20, 2021; accepted February 9, 2022 by Editorial Board Member Joanna Aizenberg

By exploring the manufacturing methods of historic objects, cultural heritage studies can yield new insights into the history of technology. The required tunability of processing steps, however, is often unknown and the underlying physics and chemistry that provide insight into the object's properties may also be lacking. A case in point is Böttger luster, a purple overglaze decoration famous for its distinctive iridescence, produced in the Meissen Manufactory from its earliest Böttger period (1710–1719) to around 1735. The iridescence of Böttger luster distinguishes it from contemporaneous purple glazes, motivating the exploration of what compositional and structural features give rise to this optical phenomenon. In this study, historic samples of Böttger luster and Purple of Cassius from Meissen are characterized and compared microscopically. The composition of both overglaze enamels is presented, including results from scanning transmission electron microscopy (STEM)-energy-dispersive X-ray spectroscopy (EDX) analyses. It was found that the iridescence and purple color of Böttger luster is due to the presence of gold nanoparticles in the glaze of the porcelain. Of specific interest is how the underlying physics of scattering and interference of the nanoparticle array is responsible for the iridescence that distinguishes Böttger luster from other gold-based purple colorants, including Purple of Cassius. Coupling these results with prior findings of Meissen porcelains, the glazes were recreated and characterized using scanning electron microscopy (SEM)-EDX, X-ray diffraction (XRD), and ultraviolet-visible spectroscopy (UV-Vis), offering insights into compositional requirements to produce purple luster.

cultural heritage science | porcelain | lusterware | gold nanoparticles

Significance

The exploration of gold-based colorants in glass and glazes led Nobel Laureate Richard Zsigmondy to the study of colloids, and to the development, with Henry Siedentopf, of the earliest microscopes capable of resolving such small length scales. Zsigmondy's studies were preceded by alchemical investigations starting in the 17th century that yielded the gold-based Purple of Cassius, and experiments in the early 18th century resulting in an unusual purple iridescent porcelain overglaze, called Böttger luster, at the Meissen Manufactory. We discuss the first nano-scale characterization of Böttger luster, its successful replication, and propose an explanation for its optical properties based on the physics of scattering and interference of nanoparticle arrays.

The story of Böttger luster starts with the ambitious avarice of a porcelain-crazed monarch: Augustus the Strong, Elector of Saxony (1694–1733). In the 17th century, Chinese porcelain was widely sought after by European aristocrats for its unrivalled delicacy and translucence. The original recipe of hard-paste porcelain, composed mostly of acicular mullite crystals and quartz grains in a glassy matrix, was closely guarded by Chinese potters for centuries, enhancing the value of this luxury product. The arcanum for porcelain was deeply coveted by European nobility along with the ability to transmute ordinary metals into gold. The latter pursuit led Augustus the Strong to summon the alchemist Johann Friedrich Böttger to his palace in Dresden in 1702, in a bold attempt to discover the formula for the philosopher's stone. Unfortunately for Böttger, the task was undeniably impossible, resulting in a series of failed experiments, unsuccessful attempts to flee, and his forceful recaptures (1).

Böttger's luck turned around in 1708, when he was able to appease Augustus the Strong by successfully producing the first Continental European hard-paste porcelain, also referred to as white gold (1, 2). In contrast to Chinese porcelain, Böttger porcelain contained high amounts of lime and low amounts of quartz, making it stronger and more resistant to thermal shock than contemporary porcelain formulations (3). The Meissen Manufactory, established in 1710 by Augustus the Strong and continuing to date, transitioned from producing calcium-rich Böttger porcelain to making potassium-rich Meissen porcelain around 1730 when feldspar replaced calcined alabaster as a flux (3, 4).

During its first decade of existence, the Meissen Manufactory struggled to produce overglaze polychrome decorations that were compatible with the high temperatures needed to fire porcelain, just over 1,350 °C (3, 5). Following countless experiments, the factory eventually became famous for developing a purple iridescent overglaze decoration known as Böttger luster (6), also referred to as the mother-of-pearl glaze, opal glaze, and (somewhat confusingly) "copper color" (5, 7), seen as the purple decoration in Fig. 1 in the cartouche surrounding the central decoration. Recent translations of historical recipes from the Meissen Manufactory reveal that the hue and iridescence of the glaze could be due to gold embedded in the top glaze layer (5, 8). The luster glaze is distinct from Purple of Cassius, a contemporaneous purple colorant used at Meissen

Author contributions: C.S.C., A.B., and K.T.F. designed research; C.S.C., Z.W.T., A.B., and S.X. performed research; C.S.C., Z.W.T., and A.B. analyzed data; and C.S.C., Z.W.T., A.B., and K.T.F. wrote the paper.

The authors declare no competing interests.

This article is a PNAS Direct Submission. A.M. is a guest editor invited by the Editorial Board.

[1]To whom correspondence may be addressed. Email: ktfaber@caltech.edu.

This article contains supporting information online at http://www.pnas.org/lookup/suppl/doi:10.1073/pnas.2120753119/-/DCSupplemental.

Published April 21, 2022.

Fig. 1. (*A*) Teapot from Meissen Porcelain Manufactory, Art Institute of Chicago 1991.1a-b. (*B*) Close-up of teapot showing Böttger luster.

to achieve hues ranging from purple to pink that is nonirides-cent and composed of gold nanoparticles well-dispersed in a tin-containing and lead-rich glassy matrix (9–11). The recipe for Böttger luster lacks tin, although it is also based on a lead-rich glassy matrix. Böttger luster also differs from colloidal gold-based glasses, glazes, and enamels with red to violet colors prepared with arsenic salts and used in Bernard Perrot's workshop, predating Meissen's polychrome wares (12, 13).

The formation of metal nanoparticles in overglaze decorations to create lustrous effects has been used by artisans since ninth century CE Mesopotamia, most prominently used in Spain and Italy from the 14th to the 16th centuries (14). The luster layer is typically applied by depositing a mixture of metal salts and oxides to the surface of a glazed ceramic and then heating the piece to 600 °C in a reducing atmosphere, achieved by adding smoking substances into the kiln that inhibit the flow of oxygen, e.g., burning wood. This process allows the metal ions to diffuse into the glaze and reduce into metal nanoparticles close to the surface. It is important to note that all previously reported examples of lusterware use mixtures of silver and copper nanoparticles to create gold- and red-colored lusters (14–20). This study specifically focuses on purple-colored luster glazes produced with gold nanoparticles.

The focus of this research is to characterize historic Böttger luster and compare this to a purple overglaze enamel produced at Meissen using Purple of Cassius. To further understand the materials and methods used in the original Meissen Manufactory we attempt to reproduce the luster-glazed porcelain. Analytical techniques such as energy-dispersive X-ray spectroscopy (EDX), X-ray diffraction (XRD), and ultraviolet-visible spectroscopy (UV-Vis) coupled with imaging methods such as scanning electron microscopy (SEM) and scanning transmission electron microscopy (STEM) are applied to provide insight into the composition and structure of the lusterware layers. Finally, we use experimentally determined size distributions of gold nanoparticles in Böttger luster and Purple of Cassius and consult models of Mie scattering and particle array interference to explain how the distribution, if properly tailored, gives rise to lusters through distinct optical effects.

Results and Discussion

Böttger Luster. Historic Böttger luster was examined by probing the cross-section of a lusterware sample (taken from a Meissen porcelain teapot, DC0508, from the study collection of the Winterthur Museum, Garden and Library), using STEM. The STEM micrograph, shown in Fig. 2*A*, reveals that Böttger luster includes an ∼0.3 to 0.8 μm thick layer, called the luster layer, containing gold nanoparticles dispersed within a lead silicate glaze, which by itself is ∼2.6 μm thick. The EDX maps seen in Fig. 2*B* show that the luster layer is rich in gold, aluminum, lead, and calcium. The gold nanoparticles are located close to the surface of the lead-rich glaze, with a wide distribution of particle sizes and nearest neighbor separations as seen in Fig. 2 *C* and *D*. The nanoparticle radius was measured using Image J (National Institutes of Health) analysis and found to be 34 ± 47 nm using number averaging. The error term represents one SD; see the *SI Appendix* for more details on the error analysis.

Underneath the lead-rich glaze seen in Fig. 2 is the clear base Böttger glaze. Apart from the gold nanoparticles, no additional pigments are present in the lead-rich glaze or the Böttger glaze. Therefore, it is likely that the luster layer alone is responsible for the color and iridescence. As defined in Fig. 2*A*, the oxide compositions of the luster layer, lead-rich layer, and Böttger glaze layer were measured quantitively using EDX and are presented in Table 1. The composition of the luster layer's lead silicate matrix is similar to the copper/pink colorant on object AR1 of Domoney et al. (9), an 18th century Meissen porcelain vase dated between 1725 and 1733 thought to be decorated with Böttger luster.

Böttger luster is closely related to other forms of lusterware caused by different metal nanoparticles, such as silver and copper (14, 18, 20–22). Importantly, tin is not present in Böttger luster as indicated by the measurements in Table 1. This makes Böttger luster distinct from another glaze colorant based on gold nanoparticles, Purple of Cassius, which is used to produce noniridescent glazes with purple and pink hues.

Purple of Cassius. In parallel with historic Böttger luster, a historic Meissen purple enamel sample (taken from a cup, DC.0510, Winterthur collection) was also examined by studying its cross-section using STEM-EDX, shown in Fig. 3 *A* and *B*. The purple enamel revealed a similar multilayered structure to Böttger luster, with a 200-nm thick layer containing gold nanoparticles. The gold nanoparticle radius is 16 ± 11 nm by number averaging, much smaller than the sizes seen in Böttger luster. The error term represents one SD. The

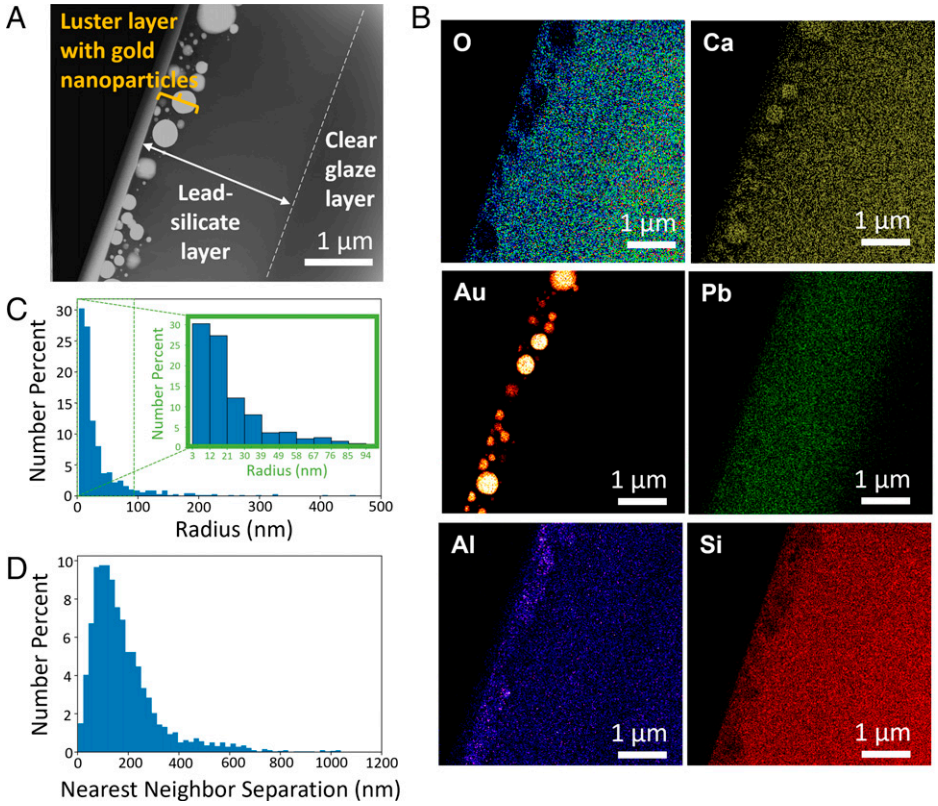

Fig. 2. (*A*) STEM image of historic Böttger luster, showing spherical Au nanoparticles near the surface. (*B*) corresponding EDX maps of several elements. (*C*) Distribution of gold nanoparticle sizes with detail included as inset. (*D*) Distribution of the nearest neighbor separation of gold nanoparticles.

homogeneous nanoparticle size distribution seen in the purple enamel sample is similar to that observed in historic Gold Ruby glass (23, 24). Bar charts showing the distribution of gold nanoparticle sizes and the distance between neighboring particles are shown in Fig. 3 *C* and *D*.

The gold nanoparticle layer is located within an ∼1-µm thick lead silicate layer. Similar to the Böttger luster, the lead-rich glaze sits over a high-temperature base glaze. The oxide compositions of the gold nanoparticle-rich region, the lead-rich layer, and the base glaze layer were measured quantitively using EDX (Fig. 3*B*) and are presented in Table 1.

The base glazes seen in the purple enamel sample and in the Böttger luster sample have similar compositions, which is expected considering that both pieces originate from the Meissen Manufactory in the 18th century. In contrast, the lead-rich glaze in the purple enamel sample is richer in PbO and CaO than the luster sample. Traces of iron are present within the glaze, which could imply the presence of small Fe_2O_3 particles that could contribute to the red tones of the purple enamel (25). However, the purple color likely originates from the gold nanoparticle-containing layer, which is also rich in aluminum, lead, calcium, and tin. Unlike Böttger luster, the gold nanoparticles in the purple enamel sample are surrounded by a tin-rich matrix. The presence of tin suggests that the gold nanoparticles had been added as Purple of Cassius, a famous purple colorant since ancient times.

Table 1. Composition (wt.%) of lead glazes and clear Böttger glazes, omitting Au content.

	Al_2O_3	SiO_2	CaO	Na_2O	K_2O	PbO	SnO_2	As_2O_3*	Other†
Historic Böttger luster layer (<800 nm)‡	13.6	61.7	2.6	0	0.1	21.7	0	0	0.3
Historic Böttger lead-rich layer (∼2.6 µm)‡	16.2	63.2	2.8	0	0.3	17.4	0	0	0.1
Copper/pink colorant from object AR1, (ref. 9)‡	8.99	60	6.79	0.73	1.65	15.4	0	0.55	5.89
Historic clear Böttger glaze (close to Pb-rich layer)	18.78	78.39	2.16	0	0.55	0	0	0	0.12
Historic clear Böttger glaze (further from Pb-rich layer)	20.71	76.23	2.59	0	0.34	0	0	0	0.13
Historic purple glaze gold layer (200–300 nm)‡	9.2	37.5	3.2	0	0.3	36.4	12.2	0	1.2
Historic purple glaze lead-rich layer (∼1 µm)‡	11.9	47.2	4	0	0.2	36	0	0	0.7
Historic purple glaze clear Böttger glaze	18.05	75.17	5.04	0	1.23	0	0	0	0.51
Reproduction lead-rich layer after firing–Baseline‡	5.4	39.6	7.3	0.3	0.5	46.8	0	0	0.1
Reproduction lead-rich layer after firing–High Ca/K‡	3.9	33.4	23.1	0.1	0.7	38.7	0	0	0.1
Reproduction lead-rich layer after firing–High Pb‡	2.6	38.6	4.2	0.4	1.2	52.9	0	0	0.1

*Spectral overlaps between the following X-ray lines make it challenging to reliably determine and quantify the presence of minor amounts of arsenic, especially considering the high quantity of gold reported by Domoney et al. for objects AR1: Mg K/As L, Pb Lα/As Kα, and Au Lβ/As Kβ.
†Other includes trace amounts of oxides of Mg, Fe, Cr, Ti, P.
‡Recalculated and normalized to exclude Au from the total, to represent the lead-rich matrix surrounding the Au nanoparticles. Note that the original reported Au content in the copper/pink colorant from object AR1 is 45.4 wt.%

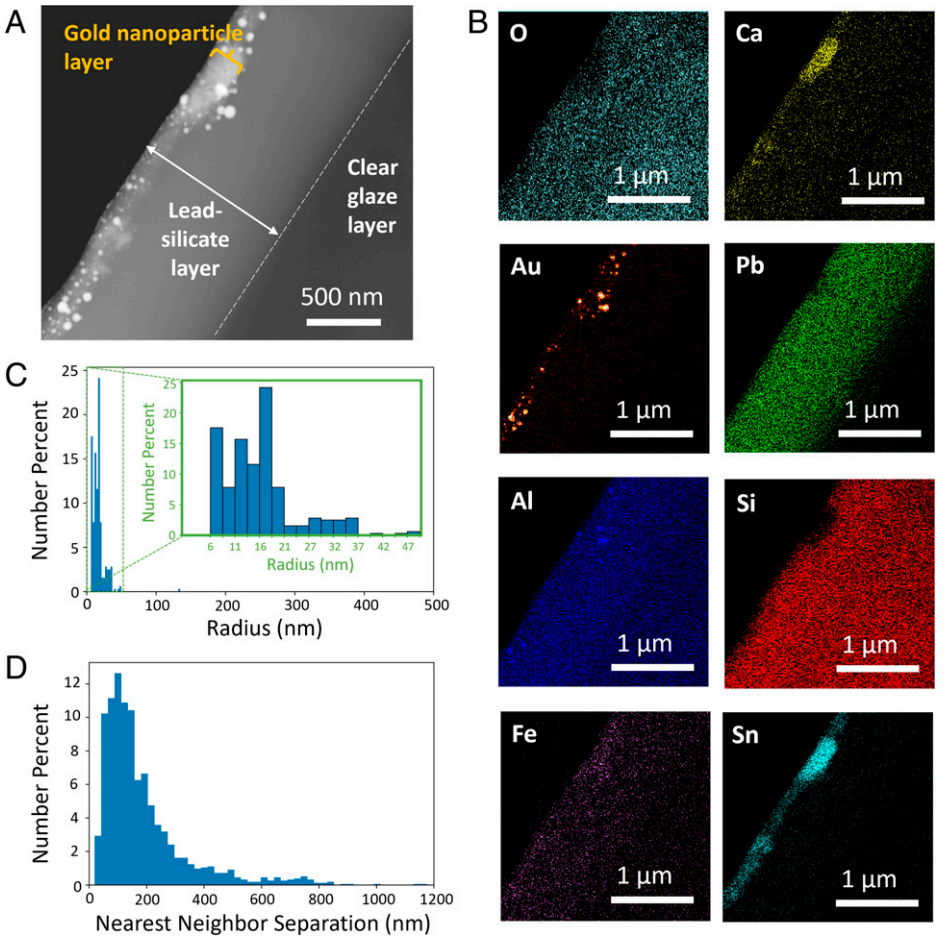

Fig. 3. (*A*) STEM image of historic Meissen purple enamel sample, showing spherical Au particles near the surface. (*B*) Corresponding EDX maps of several elements. (*C*) Distribution of gold nanoparticle sizes with detail included as inset. (*D*) Distribution of the nearest neighbor separation of gold nanoparticles.

Specifically, Purple of Cassius, a precipitate of tin(IV) oxide and colloidal gold, can be prepared using a mixture of tin(II) and tin(IV) chlorides, and gold(III) chloride, as shown by several previous studies (26–28). Tin(II) chloride serves as a reducing agent that facilitates the reduction of gold ions into metal nanoparticles (29). The gold nanoparticles pigment can be fused with glaze-making components to create purple and pink overglaze decorations (27, 30). Because such gold nanoparticles are formed prior to firing, and therefore do not require nucleation within the glaze during the firing process, they are smaller and more uniform in size and particle dispersion.

Analysis of Reproductions. Böttger porcelain and the base Böttger glaze were reproduced based on recipes by Kingery and Vandiver (3), further described and characterized in *SI Appendix*. Unlike Böttger porcelain and the Böttger glaze, there is limited information available on the lead-rich glazes used in the Meissen Manufactory in the 18th century. Lead was popularly added to lower the melting temperature of pottery glazes in this period, allowing the glaze to uniformly cover the ceramic piece by firing it at a much lower temperature than would be required for unleaded silicate-based glazes. In this study, three recipes of lead glazes were investigated, referred to as Baseline, High Ca/K and High Pb (described in *Materials and Methods*). The compositions of the lead glazes were chosen so that they could soften at the luster forming temperature of 600 °C. The oxide compositions of the fired glazes can be found in Table 1.

Recently translated records and recipes for overglaze enamels by Johann Gregorius Höroldt, who became renowned for porcelain decoration at the Viennese Du Paquier Manufactory prior to joining Meissen, reveal that the unstable explosive aurum fulminans, essentially gold(I) hydrazide, was used to introduce gold ions into the lead glaze to create the luster layer (8). Additionally, previous research suggests that a flux of powdered leaded glass was used in preparing the historic overglazes (8, 31). In this study, modifications were made to the original recipe to avoid the safety concerns associated with handling gold(I) hydrazide and processing lead-rich powders. Instead, we used a solution of gold(III) chloride, a substance readily available to Meissen workers in the 18th century, as the source of gold ions. Gold dissolves in aqua regia to form chloroauric acid ($HAuCl_4$), which dissociates into gold(III) chloride and HCl. Since gold is the most electronegative among all transition metals, gold(III) chloride or $HAuCl_4$ are readily reduced to gold at relatively low temperatures in oxygen deficient atmospheres. Furthermore, we prepared a slurry with the raw components needed to create a lead-silicate matrix, further described in *Materials and Methods*, instead of preparing and handling a frit of pretreated lead-rich powders.

Photographs of the samples, shown in Fig. 4*A*, reveal that the Baseline composition of the lead-rich glaze produced the most iridescent sample. The High Ca/K glazed sample contained regions where the metallic luster was visible, however, the luster was not as consistent as that seen with the Baseline glaze. SEM images show that both glazes contain gold nanoparticles on

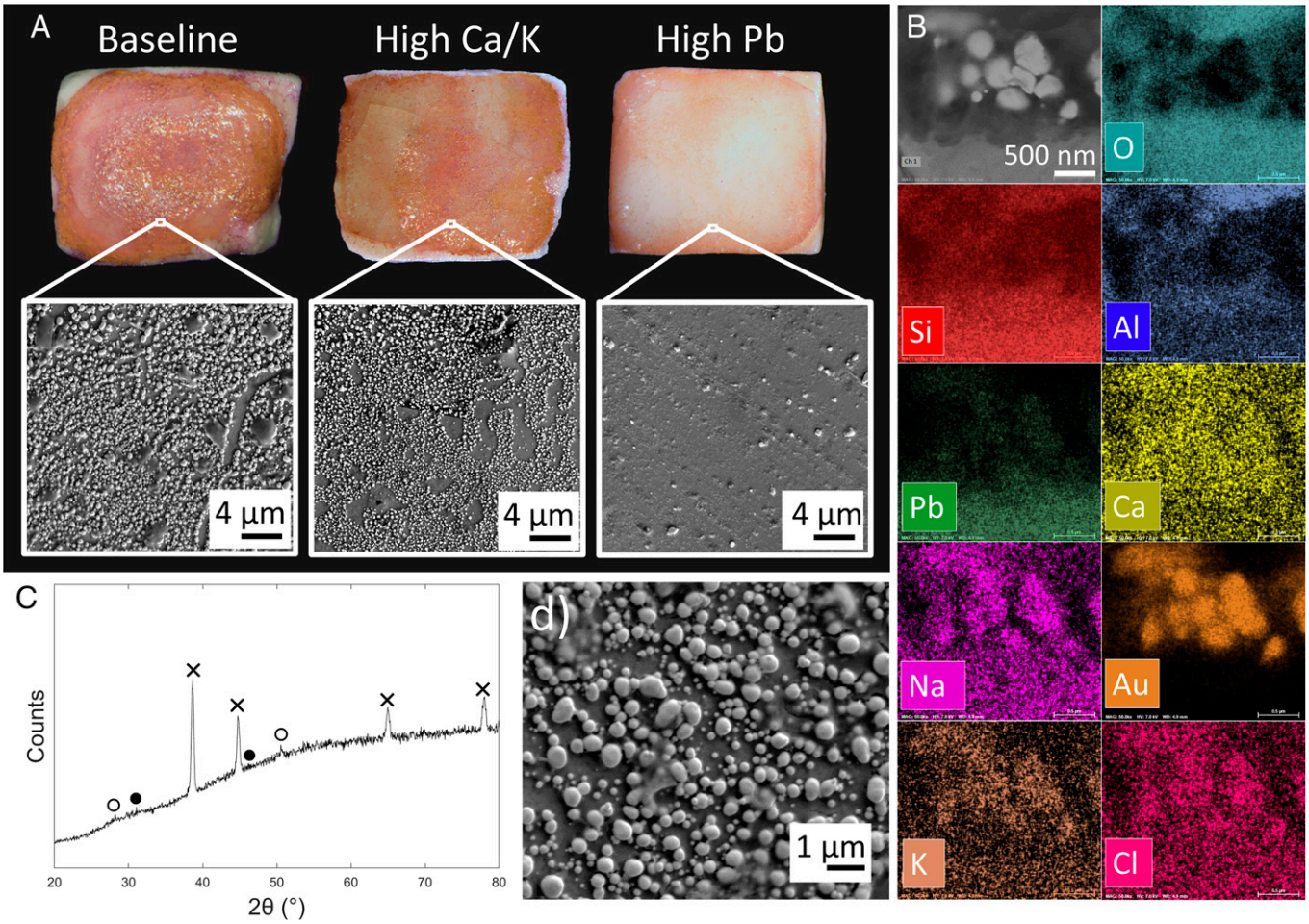

Fig. 4. (*A*) Photographs of purple luster reproductions, comparing three different compositions of the lead-silicate layer with corresponding SEM-EDX images of the surfaces of each lead glaze. (*B*) SEM-EDX images of cross-section of Baseline sample. (*C*) XRD pattern of Baseline sample indicating the presence of Au nanoparticles (×), NaCl (●) and KCl (○). (*D*) SEM images of surface of Baseline sample, showing Au nanoparticles on the surface of the luster layer.

their surface. The High Pb glazed sample, although colored pink due to the presence of gold nanoparticles, exhibited no luster from the naked eye. SEM images suggest that this could be due to the shortage of gold nanoparticles on the surface of the High Pb glaze, possibly due to the higher lead content and therefore lower melting temperature of the glaze.

The SEM-EDX maps presented in Fig. 4*B* show that the gold-containing locations within the luster layer are also rich in sodium, potassium, and chlorine. We hypothesize that the alkali ions, both K^+ and Na^+, were leached from the sanidine-type feldspar, which was a main ingredient of the lead-rich slurry (32). These alkali ions may have diffused toward the metal-bearing chloride to form KCl and NaCl salts around the gold nanoparticles. This is different from what is seen in historic Böttger luster, where the gold-source is gold (I) hydrazide and not gold (III) chloride. Nevertheless, we observe that the gold ions still reduce to metallic gold and coarsen similarly to what was seen in Böttger luster. Furthermore, the gold-free locations contain silicon, aluminum, oxygen, and traces of lead, showing that the nanoparticles are located within a PbO-SiO_2-Al_2O_3 matrix, reminiscent of what was previously seen in historic Böttger luster.

The X-ray diffraction pattern shown in Fig. 4*C* verifies that the luster glaze is composed of gold nanoparticles in a glassy matrix, with minor peaks attributed to the presence of salts. Fig. 4*D* shows a close-up of the particle array observed on the surface of the Baseline lead glaze. The average nanoparticle radius was measured to be 89 ± 52 nm using number averaging, which falls within the range observed in historic Böttger luster. The error term represents one SD. Applying the luster layer using gold(III) chloride therefore gave comparable results to the original application method using gold(I) hydrazide, ultimately producing purple luster. Despite differences in the chemistry of the matrix, we see that in both cases gold-bearing compounds can grow into gold nanoparticles of varying sizes.

Optical Effects. Nanoparticles may contribute to the coloration of a sample through several mechanisms. Plasmonic effects exist for nanoparticles under ∼15 nm in radius due to resonant oscillation of a nanoparticle's electrons with incident light waves (21, 33–35). The nanoparticles in the Böttger luster and Purple of Cassius samples are generally larger than the scale at which plasmonic effects occur. Rather, they fall into the regime of Mie scattering, which is a largely geometric effect for nanoparticles upwards of ∼15 nm that produce a purple hue (33, 36–38). In an infinite suspension of nanoparticles, this would fully describe the behavior, however, these glazes produce a structured distribution of nanoparticles in space, as well as in size. Namely, nanoparticles are localized to the surface of the glazes in an approximately uniform spatial distribution, ∼100 nm internanoparticle separation distances for both glazes (Figs. 2*D* and 3*D*). This can give rise to diffraction from a particle array, similar to that of diffraction gratings (39, 40). This phenomenon can result in luster, or iridescence, as the

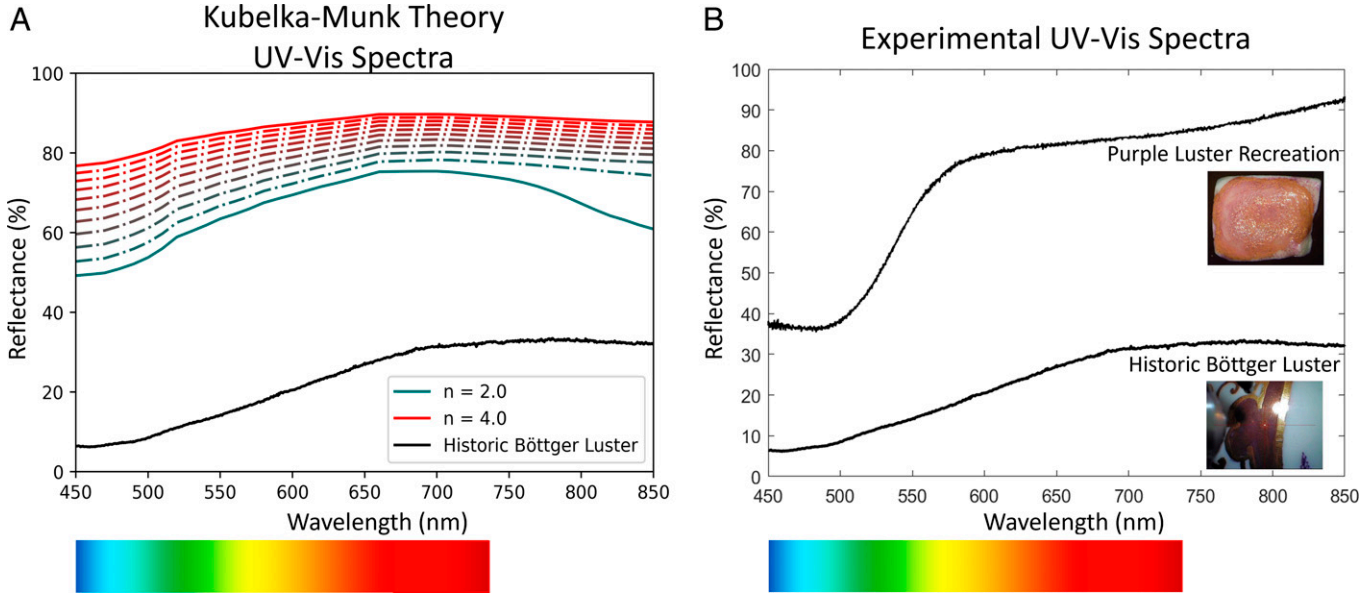

Fig. 5. (*A*) Kubelka-Munk theoretical UV-Vis spectra showing reflectance of an infinitely thick nanoparticle layer (also referred to as reflectivity) as a function of wavelength, along with the experimentally obtained UV-Vis spectrum of historic Böttger luster. (*B*) Experimental UV-Vis spectra of Böttger luster, including recreated and historic samples. Note: the intermediate lines in the theoretical plots are spaced $\Delta n = 0.2$ apart.

interaction of light with such structures is angle-dependent, giving different colors in different lighting. To understand why Böttger luster is iridescent while Purple of Cassius is not, simulations based on simple models of particle array interference were conducted using the experimentally determined nanoparticle size and spacing distributions (41).

When producing Böttger luster from gold-bearing salts, a large distribution of gold nanoparticle sizes is observed due to the occurrence of multiple nucleation sites during firing. The simulations indicated that Böttger luster is a result of the combined effects of: 1) Mie scattering of small nanoparticles (in the radius range of 15 to 250 nm) producing hue without luster and 2) disordered nanoparticle array interference of large nanoparticles (~100 nm radius) with large periodicity (on the order of several hundred nanometers) producing luster in the visible spectrum. These findings were based on the gold particle sizes seen in Fig. 2. More specifically, hue without iridescence is dominated by the Mie scattering of the many small nanoparticles of ~25 nm in radius.

Purple of Cassius is formed by mixing tin chloride with gold chloride, resulting in colloidal gold and tin oxide. The metal nanoparticles form before being applied as a colorant, resulting in controlled particle growth and better particle dispersion. As such, these small (~20 nm radius), more uniform nanoparticles produce no array interference in the visible spectrum. Instead, there is only Mie scattering of the small nanoparticles within the tin-rich layer, which produces a color without any lustrous effect. These findings were based on the gold particle sizes seen in Fig. 3. With this knowledge, a successful lustrous reproduction would be expected to have a polydisperse distribution of gold nanoparticles, with enough gold content to nucleate large nanoparticles and many smaller ones near the surface, but not so high as to create a thick film of gold, as is seen in gilding.

Shown in Fig. 5*A*, simulations of the hue, based on Kubelka-Munk theory, were compared to the UV-Vis reflectance spectrum of historic Böttger luster. Spectra are displayed for indices of refraction (n) ranging between $2 < n < 4$, to illustrate how small deviations of the refractive index of the lead-rich matrix can influence the reflectivity of the glaze. Our results align with the empirical observation that nanoparticles in the radius range of ~15 to 250 nm produce a purple coloration. Resonant reflectance can occur at wavelengths slightly larger than the array's periodicity, with smaller nanoparticles giving sharper peaks (41). Therefore, Böttger luster's very largest nanoparticles, which are widely separated, create broad peaks in the visible reflectance spectrum, generating luster in addition to the underlying coloration from Mie scattering. Conversely, the smaller nanoparticles (less than 15 nm), which have much smaller periodicity, produce narrow peaks in the UV reflectance spectra and do not contribute to visible optics.

UV-Vis was also used to compare a historic sample of Böttger luster to our purple luster recreation, seen in Fig. 5*B*. Experimental results are consistent with the observed colors of the glazes, where our purple reproduction strongly reflects red-yellow with traces of green and blue, while the darker purple of the historic Böttger luster sample reflects more blue light. The reproduction is more reflective than the historic sample, possibly because the lead glaze of the recreation contains 46.8 wt.% PbO while the historic sample contains 21.7 wt.% PbO. In fact, the reflectivity of pure PbO increases dramatically around 500 nm wavelength, which could account for the sharp increase in reflectance observed in the purple luster reproduction at that wavelength (42). Our results suggest that the optical properties of Böttger luster are governed by the highly reflective, gold-containing lead glaze, and have little to do with the underlying clear Böttger glaze and porcelain body.

Conclusion

By characterizing historic samples of Böttger luster, we confirmed experimentally that the iridescence and purple color of Böttger luster originates from an array of gold nanoparticles situated near the surface of the glazed porcelain. This was validated using models of Mie scattering and disordered nanoparticle array interference. Böttger luster exhibits metallic sheen as well as iridescence despite only containing a single layer of nanoparticles, unlike silver- and copper-based lusterware that have multiple bands of nanoparticles separated by a glassy region.

Böttger luster was compared to Purple of Cassius, a more frequently used purple colorant, composed of colloidal gold within a tin-rich glassy matrix. STEM-EDX analyses of cross-sections of Böttger luster and Purple of Cassius glazes reveal information on how the gold nanoparticles are created and distributed within each glaze, implying vital differences between their application methods. In Böttger luster, as with other types of lusterware, the metal nanoparticles develop in the top glaze through a firing step that allows metal ions to diffuse, nucleate and grow into particles of several sizes inside the glaze. In Purple of Cassius, the gold nanoparticles are precipitated using tin(II) chloride prior to being incorporated into the leaded frit that is applied to create an overglaze enamel, providing a more homogenous particle dispersion and smaller particle sizes.

Purple luster was created through the evaluation of three lead glazes, and analyzed using SEM-EDX, XRD, and UV-Vis. It was determined that the iridescent reproductions contain gold nanoparticles in a lead glaze, like the structure seen in historic Böttger luster. Thus, we have demonstrated that purple luster can be produced following modern-day safety standards, applying gold(III) chloride as the source of gold ions along with minimal processing of lead-rich powders, albeit with the formation of alkali salts in a matrix that is chemically different from historic Böttger luster.

The techniques used by alchemists in the 18th century Meissen Manufactory were likely the fruit of repeated trials in their tireless attempts to appease Augustus the Strong. Yet, with the aid of contemporary scientific analytical and imaging techniques, we have revealed that the purple colorants of Meissen owe their color and shine to the hidden chemistry, kinetics, and optical effects occurring in their decorative glazes.

Materials and Methods

Characterization of the Historic Meissen Samples and Reproductions. Fragments (0.5 × 0.5 mm) of decorative surface layers were obtained from Meissen porcelain dated to the 18th century. Two gold-containing decorative samples were studied: one was a lustrous sample from a Meissen porcelain teapot (DC.0508, from the study collection of the Winterthur Museum, Garden and Library, 18th century) and the other a piece of purple enamel from a cup (DC.0510, Winterthur collection, 18th century).

Transmission electron microscopy (TEM) samples were prepared with focused ion beam (FIB). Cross-sectional slices with electron transparency were extracted from the purple regions, revealing the multilayered structure of the surface decoration. The distribution of nanoparticles as well as the glaze chemistry were determined via STEM (JEOL JEM-2100 FasTEM). The operating voltage was 200 kV. The chemistry of the glaze was studied using EDX coupled with the STEM. INCA software was used for EDX acquisition and analysis.

Reproductions were analyzed using an array of imaging and chemical characterization methods. A camera was used to capture the iridescence of the samples at the macroscale (Nikon D7500, AF-S Micro Nikkor 40mm Lens, Nikon). The surface microstructure and overview cross-section of the lusterware samples were imaged using SEM (ZEISS 1550VP FESEM, Carl Zeiss Microscopy GmbH). The elemental compositions of the individual layers were determined using energy dispersive X-ray spectroscopy (Oxford X-Max SDD X-ray Energy Dispersive Spectrometer). The cross-section of the luster layer was imaged using SEM (Nova 200 NanoLab, Thermo Fisher) and the elemental compositions were determined using EDX (Bruker Quantax X-ray Energy Dispersive Spectrometer). The chemical composition of the reproduced Böttger porcelain and purple luster layer was measured using XRD (Panalytical X'Pert Prodiffractometer) with a Cu source at 45 kV and 40 mA, scanned from 20° to 80° 2θ.

UV-Vis of the historic Böttger luster sample was carried out with a normal illumination/normal collection setup using a 200-μm diameter single fiber illumination leg and a single fiber collection leg of the same diameter (Ocean Optics BIF200-UV/VIS), a halogen light source (Ocean Optics DH-2000-BAL), and an Ocean Optics spectrometer (OCEAN-FX-XR1-ES, XR1-500 line/mm grating blazed at 250 nm) to collect 20 averaged spectra, each at 1,000-ms collection time, controlled by OceanView software. For the recreation sample, a normal illumination/normal collection setup was used using a 400-μm diameter 6-fiber illumination leg and a single fiber collection leg of the same diameter (Ocean Insight QR400-7-SR-BX), a halogen light source, a Shamrock spectrometer (SR-193i-B2, S/N SR-2502), and a silicon CCD Camera (IDUS D4420A-OE, S/N CCD-19533, May 2016) to collect spectra controlled by Andor Solis software.

Table 2. Raw materials (g) used in lead-rich glaze reproductions.

	Baseline	High Ca/K	High Pb
Quartz	0.40	0	0
Feldspar	1	1.60	0.57
Clay	0.68	0.16	0.15
Calcium carbonate	1	1.10	0.44
Lead bisilicate	6	5.40	7

Production of Purple Lusters. Details of the recipes used to create Böttger porcelain and the Böttger base glaze can be found in *SI Appendix*. For the luster glaze, modifications were made from the original Böttger recipe (5, 8) to avoid working with gold(I) hydrazide. First, a lead-rich glaze slurry was prepared from raw materials, including lead bisilicate (US Pigment Corporation), kaolinite (Sigma-Aldrich), potash feldspar (Custer), calcium carbonate (Alfa Aesar) and quartz (Sigma-Aldrich), which were suspended in water and ball-milled for 2 h. Table 2 summarizes the raw materials used to create all three lead-rich glazes. Exact oxide compositions of the fired glazes can be found in Table 1.

The raw slurry was then applied with a brush as a thin layer of less than 25 μm on the surface of the previously base-glazed porcelain. The freshly glazed piece was then fired at 900 °C for 2 h in air with a ramp rate of 2 °C/min. The melting point of the lead-rich layer was designed to be below 1,100 °C to avoid any intermixing between this layer and the base glaze (which begins to soften at 1,100 °C). Previous studies on lead oxide-alumina-silica glazes have reported that additions of PbO can lower the melting temperature of the system (43). Three compositions of the lead-rich glaze were investigated, referred to as: Baseline (based on STEM-EDX results of historic Meissen samples, modified so that it could begin to melt at 600 °C), High Ca/K (a Ca-rich version of Baseline), and High Pb (a Pb-rich version of Baseline). Details of their compositions are outlined in *SI Appendeix*, Table S3. The three variations each produced a clear and smooth surface after firing, and were rich in silicon, calcium, and lead. The thickness of the applied lead-rich glaze played a critical role in obtaining the correct color and luster. Applying layers less than 25 μm was desired to avoid the growth of silica or mullite crystals within the lead-rich glaze, which could alter the optical properties of the glaze.

To introduce gold ions into the glaze, an aqueous solution of gold(III) chloride was applied to the fired lead-rich glaze. The piece was then heated to 600 °C with a ramp rate of 2 °C/min, and held at that temperature for 30 min with flowing argon gas, creating an inert atmosphere. The lead-rich glazes start to soften at this temperature, facilitating the diffusion of the gold ions into the glaze where they are reduced to produce gold nanoparticles.

Spectroscopic Simulations of Lusters. Evaluating the effects of Mie scattering involved the solution of the Maxwell equations around spherical particles by expanding the problem in an infinite series of spherical harmonics (44, 45). While this provided an analytical solution, numerical approximations were necessary to evaluate that solution, and Python scripts such as PyMieScatt (37) were used to evaluate the extinction, absorption, and scattering efficiencies of nanoparticles both individually and in a size-density distribution. Kubelka-Munk theory (36) was then used to approximate the scattering and reflectivity of a suspension of nanoparticles of infinite thickness from the coefficients given by PyMieScatt (36, 37). This process is summarized in Fig. 6 to approximate the matte color purely due to the nanoparticles in a hypothetical infinite suspension and not their layered distribution. The absorption and scattering coefficients of the material, K and S, respectively, are based on the nanoparticle density and properties of the material. More precisely, they are defined as:

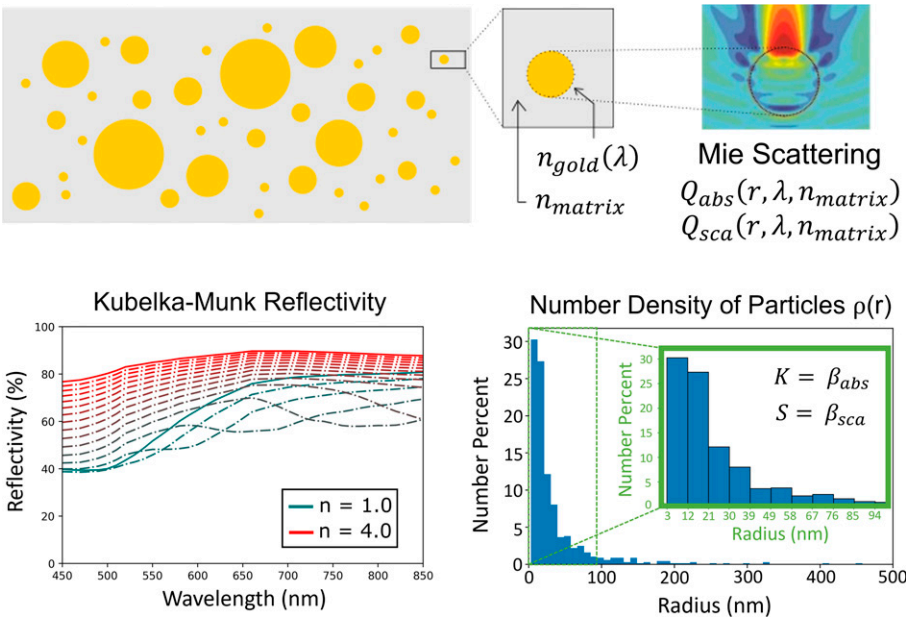

Fig. 6. Graphic summary of how the Kubelka-Munk model was computed, using experimental nanoparticle distributions and Mie scattering data.

$$K = \beta_{abs} = \int_0^\infty \pi r^2 Q_{abs}(r, \lambda, n_{matrix}) \rho(r) dr \quad [1]$$

$$S = \beta_{sca} = \int_0^\infty \pi r^2 Q_{sca}(r, \lambda, n_{matrix}) \rho(r) dr \quad [2]$$

where r is the metal nanoparticle radius, $Q_{abs}(r, \lambda, n_{matrix})$ and $Q_{sca}(r, \lambda, n_{matrix})$ are the Mie absorption and scattering coefficients, respectively, and $\rho(r)$ is the volume density describing the concentration of nanoparticles in the glassy matrix.

The reflectivity of a suspension of nanoparticles of infinite thickness is then defined as:

$$R_\infty = \frac{K + S - \sqrt{(K+S)^2 - S^2}}{S} \quad [3]$$

Approximating the disordered periodic structure of the nanoparticles as a perfect 2D square array of identical lossy particles, subjected to normal incidence of light, we applied the approach proposed by Garcia de Abajo (41) to model the luster; effectively this is the wavelength at which intensely reflective resonances occur from a uniform lattice with well-defined particle size and periodicity.

$$R = |r|^2 \quad [4]$$

$$r = \frac{\frac{2\pi i k}{A}}{\frac{1}{\alpha_E} - G_{xx}(0)} \quad [5]$$

$$\frac{1}{\alpha_E} = \frac{1}{\alpha_E^{es}} - \frac{2ik^3}{3} \quad [6]$$

$$\alpha_E^{es} = b^3 \frac{\varepsilon - 1}{\varepsilon + 2} \quad [7]$$

$$G_{xx}(0) a^3 \approx \frac{4\pi^2 \sqrt{2}}{\sqrt{\lambda/a - 1}} - 118 \quad [8]$$

In this model, the periodicity is a, nanoparticle radius is b, and the nanoparticle's complex permittivity is a constant ε. With these parameters, $A = a^2$ the area of the lattice unit cell, and the magnitude of the light wavevector k, the reflection coefficient r and thus reflectance R can be calculated. Note that introducing disorder into this system, as is more realistic, would broaden and decrease the intensity of the resonant peaks in the reflectance spectra, but would not eliminate them (41, 46, 47).

Data Availability Spectroscopy, X-ray diffraction, and electron microscopy data have been deposited in [CaltechDATA].

ACKNOWLEDGMENTS. We thank Jennifer L. Mass (Scientific Analysis of Fine Art, LLC., and Bard Graduate Center, previously Winterthur Museum, Garden and Library) and Leslie Grigsby (Senior Curator of Ceramics and Glass, Winterthur Museum, Garden and Library) for providing us with historic Böttger and Meissen porcelain fragments from Winterthur's study collection, which allowed the sample-based characterization of Böttger luster and purple overglaze enamel layers. Funding supporting the replication of Meissen porcelain bodies, Böttger luster, and for luster characterization at Northwestern University was provided by an Art Institute of Chicago–Northwestern University Exploratory Research Grant (2008–2009). This work made use of the EPIC facility of Northwestern University's NUANCE Center, which has received support from the SHyNE Resource (NSF ECCS-2025633), the IIN, and Northwestern's MRSEC program (NSF DMR-1720139). The authors gratefully acknowledge Zun Chen and Andrew Azman for their preliminary research on recreating Böttger glazes. Additionally, the authors thank Rebecca Gallivan and Miguel Caban-Acevedo from Caltech, for their interest in the project and advice on imaging techniques, as well as Prof. George Rossman from Caltech for his helpful insights on collecting UV-Vis data of iridescent materials.

Author affiliations: [a]Division of Engineering and Applied Science, California Institute of Technology, Pasadena, CA 91125; [b]Institute for the Preservation of Cultural Heritage, Yale University, West Haven, CT 06516; and [c]Department of Materials Science and Engineering, Northwestern University, Evanston, IL 60208

1. J. Gleeson, *The Arcanum: The Extraordinary True Story* (Warner Books, Inc.) 1998.
2. M. Spataro, N. Meeks, M. Bimson, A. Dawson, J. Ambers, Early porcelain in seventeenth-century England: Non-destructive examination of two jars from Burghley House. *The British Museum Technical Research Bulletin* **3**, 37–46 (2009).
3. W. D. Kingery, P. B. Vandiver, *Ceramic Masterpieces* (The Free Press) 1986.
4. A. Bezur, F. Casadio, "Du Paquier porcelain: Artistic expression and technological mastery. A scientific evaluation of the materials" in *Fired by Passion. Vienna Baroque Porcelain of Claudius Innocentius Du Paquier*, M. Chilton, Ed. (Arnoldsche, 2009), p. 1204.
5. N. Zumbulyadis, … with a dreadful bang" - A chemical history of Boettger lustre. *Keramos* **222**, 3–16 (2013).
6. D. Lübke, Böttger-Lüster. *Keramos* **185**, 13–22 (2004).
7. R. Seyffarth, Johann Gregor Höroldt als Chemiker und Techniker. *Mitteilungsblatt/Keramik-Freunde der Schweiz* **39** (1957).
8. N. Zumbulyadis, Decorating with explosives: The use of aurum fulminans as a purple pigment. *Bull. Hist. Chem.* **39**, 7–17 (2014).
9. K. Domoney, A. J. Shortland, S. Kuhn, Characterization of 18th-century Meissen porcelain using SEM-EDS. *Archaeometry* **54**, 454–474 (2012).
10. F. Casadio *et al.*, X-ray fluorescence applied to overglaze enamel decoration on eighteenth- and nineteenth-century porcelain from central Europe. *Stud. Conserv.* **57**, S61–S72 (2012).
11. N. Zumbulyadis, V. Van Thienen, Changes in the body, glaze and enamel compositions of early Meissen porcelain, 1723–c.1740. *Archaeometry* **62**, 22–41 (2020).

12. P. Colomban *et al.*, Investigation of the pigments and glassy matrix of painted enamelled qing dynasty chinese porcelains by noninvasive on-site raman microspectrometry. *Heritage* **3**, 915–940 (2020).
13. C. Louis, O. Pluchery, "Gold nanoparticles in the past: Before the nanotechnology era" in *Gold Nanoparticles for Physics, Chemistry and Biology*, C. Louis, O. Pluchery, Eds. (Imperial College Press, 2012), pp. 13–17.
14. I. Borgia *et al.*, Characterisation of decorations on Iranian (10th–13th century) lustreware. *Appl. Phys. A Mater. Sci. Process.* **79**, 257–261 (2004).
15. P. Colomban, The use of metal nanoparticles to produce yellow, red and iridescent colour, from bronze age to present times in lustre pottery and glass: Solid state chemistry, spectroscopy and nanostructure. *J Nano Res* **8**, 109–132 (2009).
16. I. Borgia *et al.*, Heterogeneous distribution of metal nanocrystals in glazes of historical pottery. *Appl. Surf. Sci.* **185**, 206–216 (2002).
17. P. Fredrickx, D. Hélary, D. Schryvers, E. Darque-Ceretti, A TEM study of nanoparticles in lustre glazes. *Appl. Phys. A Mater. Sci. Process.* **79**, 283–288 (2004).
18. J. Molera, M. Mesquida, J. Perez-Arantegui, T. Pradell, M. Vendrell, Lustre recipes from a Medieval workshop in Paterna. *Archaeometry* **43**, 455–460 (2001).
19. G. Padeletti, P. Fermo, Production of gold and ruby-red lustres in Gubbio (Umbria, Italy) during the Renaissance period. *Appl. Phys. A Mater. Sci. Process.* **79**, 241–245 (2004).
20. S. Padovani *et al.*, XAFS study of copper and silver nanoparticles in glazes of medieval middle-east lustreware (10th–13th century). *Appl. Phys. A Mater. Sci. Process.* **83**, 521–528 (2006).
21. J. Lafait, S. Berthier, C. Andraud, V. Reillon, J. Boulenguez, Physical colors in cultural heritage: Surface plasmons in glass. *C. R. Phys.* **10**, 649–659 (2009).
22. G. Padeletti, P. Fermo, Italian Renaissance and Hispano-Moresque lustre-decorated majolicas: Imitation cases of Hispano-Moresque style in central Italy. *Appl. Phys. A Mater. Sci. Process.* **77**, 125–133 (2003).
23. M. Verita, P. Santopadre, Analysis of gold-colored Ruby Glass tesserae in Roman church mosaics of the 4th to 12th centuries. *J. Glass Stud.* **52**, 11–24 (2010).
24. F. E. Wagner *et al.*, Before striking gold in gold-ruby glass. *Nature* **407**, 691–692 (2000).
25. F. Gol, *et al.*, Coloring effect of iron oxide content on ceramic glazes and their comparison with the similar waste containing materials. *Ceramics Int.* **48**, 2241–2249 (2021).
26. L. B. Hunt, The true story of Purple of Cassius: The birth of gold-based glass and enamel colours. *Gold Bull.* **9**, 134–139 (1976).
27. W. D. Kingery, P. B. Vandiver, "The 18th century changes in technology and style from the Famille Verte palette to the Famille Rose palette" in *Ceramics and Civilization: Technology and Style, Vol. 2*, W.D. Kingery, Ed. (The American Ceramic Society, 1986), pp. 363–382.
28. A. Ruivo *et al.*, Gold nanoparticles in ancient and contemporary ruby glass. *J. Cult. Herit.* **9**, 134–137 (2008).
29. S. Haslbeck, K. P. Martinek, L. Stievano, F. E. Wagner, Formation of gold nanoparticles in gold ruby glass: The influence of tin. *Hyperfine Interact.* **165**, 89–94 (2005).
30. M. E. F. Reboulleau, M. D. Magnier, A. Romain, H. Bertran, *Nouveau Manuel Complet de la Peinture sur Verre, sur Porcelaine et sur Email* (L. Mulo, 1900).
31. D. Lübke, *Keramische Fachbegriffe für die Analyse von frühem Meissner Porzellan* (Rach Verlag Bramsche, 2014).
32. E. Menendez, R. Garcia-Roves, B. Aldea, Incidence of Alkali release in concrete dams. Evaluation of Alkalis releasable by Feldspars. *MATEC Web Conf.* 199, 03006 (2018).
33. P. Mulvaney, Not all that's gold does glitter. *MRS Bull.* **26**, 1009–1014 (2001).
34. L. Novotny, B. Hecht, "Surface plasmons" in *Principles of Nano-Optics*, (Cambridge University Press, 2006), pp. 369–413.
35. Humboldt-Universität zu Berlin, Plasmonics. https://www.physik.hu-berlin.de/de/nano/lehre/Gastvorlesung%20Wien/plasmonics. Accessed 4 April 2022.
36. H. G. Hecht, The interpretation of diffuse reflectance spectra. *J. Res. Natl. Bur. Stand. A Phys. Chem.* **80A**, 567–583 (1976).
37. B. Sumlin, Functions for Forward Mie Calculations of Homogeneous Spheres–PyMieScatt 1.7.5 documentation.
38. X. Fan, W. Zheng, D. J. Singh, Light scattering and surface plasmons on small spherical particles. *Light Sci. Appl.* **3**, 1–14 (2014).
39. V. Reillon, S. Berthier, C. Andraud, Optical properties of lustred ceramics: Complete modelling of the actual structure. *Appl. Phys. A Mater. Sci. Process.* **100**, 901–910 (2010).
40. H. Hirayama, K. Kaneda, H. Yamashita, Y. Monden, An accurate illumination model for objects coated with multilayer films. *Comput. Graph.* **25**, 391–400 (2001).
41. F. J. García de Abajo, Colloquium: Light scattering by particle and hole arrays. *Rev. Mod. Phys.* **79**, 1267–1290 (2007).
42. S. Zou *et al.*, A new reaction between common compounds: Lead oxide reacts with formaldehyde. *Chem. Commun. (Camb.)* **50**, 6316–6318 (2014).
43. R. F. Geller, E. N. Bunting, Report on the systems lead oxide-alumina and lead oxide- alumina-silica. *J. Res. Natl. Bur. Stand.* **31**, 255–270 (1943).
44. A. Chhatre, P. Solasa, S. Sakle, R. Thaokar, A. Mehra, Color and surface plasmon effects in nanoparticle systems: Case of silver nanoparticles prepared by microemulsion route. *Colloids Surf. A Physicochem. Eng. Asp.* **404**, 83–92 (2012).
45. W. J. Wiscombe, Improved Mie scattering algorithms. *Appl. Opt.* **19**, 1505–1509 (1980).
46. D. Pacifici, H. J. Lezec, L. A. Sweatlock, R. J. Walters, H. A. Atwater, Universal optical transmission features in periodic and quasiperiodic hole arrays. *Opt. Express* **16**, 9222–9238 (2008).
47. F. Przybilla, C. Genet, T. W. Ebbesen, Long vs. short-range orders in random subwavelength hole arrays. *Opt. Express* **20**, 4697–4709 (2012).